Received 24 June; accepted 8 September 2003; doi:10.1038/nature02030.
Published online 21 September 2003.

1. Badano, J. L. *et al.* Identification of a novel Bardet-Biedl syndrome protein, BBS7, that shares structural features with BBS1 and BBS2. *Am. J. Hum. Genet.* **72,** 650–658 (2003).
2. Slavotinek, A. M. *et al.* Mutations in MKKS cause Bardet-Biedl syndrome. *Nature Genet.* **26,** 15–16 (2000).
3. Katsanis, N. *et al.* Mutations in MKKS cause obesity, retinal dystrophy and renal malformations associated with Bardet-Biedl syndrome. *Nature Genet.* **26,** 67–70 (2000).
4. Nishimura, D. Y. *et al.* Positional cloning of a novel gene on chromosome 16q causing Bardet-Biedl syndrome (BBS2). *Hum. Mol. Genet.* **10,** 865–874 (2001).
5. Mykytyn, K. *et al.* Identification of the gene (*BBS1*) most commonly involved in Bardet-Biedl syndrome, a complex human obesity syndrome. *Nature Genet.* **31,** 435–438 (2002).
6. Mykytyn, K. *et al.* Identification of the gene that, when mutated, causes the human obesity syndrome BBS4. *Nature Genet.* **28,** 188–191 (2001).
7. Beales, P. L. *et al.* Genetic interaction of BBS1 mutations with alleles at other BBS loci can result in non-Mendelian Bardet-Biedl syndrome. *Am. J. Hum. Genet.* **72,** 1187–1199 (2003).
8. Katsanis, N. *et al.* Triallelic inheritance in Bardet-Biedl syndrome, a mendelian recessive disorder. *Science* **293,** 2256–2259 (2001).
9. Badano, J. L. & Katsanis, N. Beyond Mendel: an evolving view of human genetic disease transmission. *Nature Rev. Genet.* **3,** 779–789 (2002).
10. Katsanis, N. *et al. BBS4* is a minor contributor to Bardet-Biedl syndrome and may also participate in triallelic inheritance. *Am. J. Hum. Genet.* **71,** 22–29 (2002).
11. Maurer, L. & Orndorff, P. E. Identification and characterization of genes determining receptor binding and pilus length of *Escherichia coli* type 1 pili. *J. Bacteriol.* **169,** 640–645 (1987).
12. Merz, A. J., So, M. & Sheetz, M. P. Pilus retraction powers bacterial twitching motility. *Nature* **407,** 98–102 (2000).
13. Nonaka, S. *et al.* Randomization of left-right symmetry due to loss of nodal cilia generating leftward flow of extraembryonic fluid in mice lacking KIF3B motor protein. *Cell* **95,** 829–837 (1998).
14. Dammermann, A. & Merdes, A. Assembly of centrosomal proteins and microtubule organization depends on PCM-1. *J. Cell Biol.* **159,** 255–266 (2002).
15. Kubo, A., Sasaki, H., Yuba-Kubo, A., Tsukita, S. & Shiina, N. Centriolar satellites: Molecular characterization, ATP-dependent movement toward centrioles and possible involvement in ciliogenesis. *J. Cell Biol.* **147,** 969–979 (1999).
16. Rosenbaum, J. L. & Witman, G. B. Intraflagellar transport. *Nature Mol. Cell Biol.* **3,** 813–825 (2002).
17. Haycraft, C. J., Swoboda, P., Taulman, P. D., Thomas, J. H. & Yoder, B. K. The *C. elegans* homolog of the murine cystic kidney disease gene *Tg737* functions in a ciliogenic pathway and is disrupted in *osm-5* mutant worms. *Development* **128,** 1493–1505 (2001).
18. Fujiwara, M., Ishihara, T. & Katsura, I. A novel WD40 protein, CHE-2, acts cell-autonomously in the formation of *C. elegans* sensory cilia. *Development* **126,** 4839–4848 (1999).
19. Swoboda, P., Adler, H. T. & Thomas, J. H. The RFX-type transcription factor DAF-19 regulates sensory neuron cilium formation in *C. elegans*. *Mol. Cell* **5,** 411–421 (2000).
20. Okada, Y. *et al.* Abnormal nodal flow precedes situs inversus in iv and inv mice. *Mol. Cell* **4,** 459–468 (1999).
21. Pazour, G. J. *et al.* The intraflagellar transport protein, IFT88, is essential for vertebrate photoreceptor assembly and maintenance. *J. Cell Biol.* **157,** 103–113 (2002).
22. Marszalek, J. R. *et al.* Genetic evidence for selective transport of opsin and arrestin by kinesin-II in mammalian photoreceptors. *Cell* **102,** 175–187 (2000).
23. Nauli, S. M. *et al.* Polycystins 1 and 2 mediate mechanosensation in the primary cilium of kidney cells. *Nature Genet.* **33,** 129–137 (2003).
24. Hou, X. *et al.* Cystin, a novel cilia-associated protein, is disrupted in the *cpk* mouse model of polycystic kidney disease. *J. Clin. Invest.* **109,** 533–540 (2002).
25. Morgan, D. *et al.* Expression analyses and interaction with the anaphase promoting complex protein Apc2 suggest a role for inversin in primary cilia and involvement in the cell cycle. *Hum. Mol. Genet.* **15,** 3345–3350 (2002).
26. Watanabe, D. *et al.* The left-right determinant Inversin is a component of node monocilia and other 9 + 0 cilia. *Development* **130,** 1725–1734 (2003).
27. Beales, P. L., Elcioglu, N., Woolf, A. S., Parker, D. & Flinter, F. A. New criteria for improved diagnosis of Bardet-Biedl syndrome: results of a population survey. *J. Med. Genet.* **36,** 437–446 (1999).
28. Hobert, O. PCR fusion-based approach to create reporter gene constructs for expression analysis in transgenic *C. elegans*. *Biotechniques* **32,** 728–730 (2002).
29. Brenner, S. The genetics of *Caenorhabditis elegans*. *Genetics* **77,** 71–94 (1974).

Supplementary Information accompanies the paper on **www.nature.com/nature**.

Acknowledgements We thank all the BBS families for their willing and continued participation in our studies; J. Sowden, S. Darling and R. Graham for technical help; and J. Lupski, A. Chakravarti, J. Nathans, P. Scambler, A. McCallion and L. Kotch for their critical evaluation of this manuscript. We also thank J. Morton for clinical details and J. Goodship for discussions. This study was supported by grants from the National Institute of Child Health and Development, NIH and the March of Dimes (N.K.), the Research Department of the King Khaled Eye Specialist Hospital, Riyadh, Saudi Arabia (J.C.C., R.A.L.), the Foundation Fighting Blindness, USA (R.A.L.), the Research to Prevent Blindness, New York (R.A.L.), NCIC, HSFBC&Y, CIHR and MSFHR (M.R.L.), NSERC (R.C.J.), Genome BC and Genome Canada (R.C.J., K.M.), the National Kidney Research Fund (B.E.H.), the Birth Defects Foundation (P.L.B.), and the Wellcome Trust (P.L.B.).

Authors' contributions The laboratories of M.R.L., P.L.B. and N.K. contributed equally to this work.

Competing interests statement The authors declare that they have no competing financial interests.

Correspondence and requests for materials should be addressed to N.K. (katsanis@jhmi.edu).
Nucleotide sequences for the two *BBS8* splice isoforms (AY366523 (long isoform) and AY366524 (short isoform)) have been deposited in GenBank.

The Wnt/β-catenin pathway regulates cardiac valve formation

Adam F. L. Hurlstone*, Anna-Pavlina G. Haramis*, Erno Wienholds, Harry Begthel, Jeroen Korving, Fredericus van Eeden, Edwin Cuppen, Danica Zivkovic, Ronald H. A. Plasterk & Hans Clevers

Netherlands Institute for Developmental Biology, Hubrecht Laboratory and Centre for Biomedical Genetics, Uppsalalaan 8, 3584 CT, Utrecht, The Netherlands

* These authors contributed equally to this work

Truncation of the tumour suppressor adenomatous polyposis coli (Apc) constitutively activates the Wnt/β-catenin signalling pathway[1]. Apc has a role in development: for example, embryos of mice with truncated Apc do not complete gastrulation[2]. To understand this role more fully, we examined the effect of truncated Apc on zebrafish development. Here we show that, in contrast to mice, zebrafish do complete gastrulation. However, mutant hearts fail to loop and form excessive endocardial cushions. Conversely, overexpression of Apc or Dickkopf 1 (Dkk1), a secreted Wnt inhibitor[3], blocks cushion formation. In wild-type hearts, nuclear β-catenin, the hallmark of activated canonical Wnt signalling[4], accumulates only in valve-forming cells, where it can activate a Tcf reporter. In mutant hearts, all cells display nuclear β-catenin and Tcf reporter activity, while valve markers are markedly upregulated. Concomitantly, proliferation and epithelial–mesenchymal transition, normally restricted to endocardial cushions, occur throughout the endocardium. Our findings identify a novel role for Wnt/β-catenin signalling in determining endocardial cell fate.

Apc is an essential component of the axin-containing destruction complex that phosphorylates β-catenin, tagging it for ubiquitination and degradation by the proteasome. In the presence of a Wnt ligand, β-catenin is stabilized and accumulates in the nucleus where it binds and activates Tcf transcription factors[1]. APC mutations, common in colorectal cancer, occur proximal to the axin-binding motifs in the mutation cluster region (MCR; Fig. 1a). These truncations lead to constitutive activation of the pathway.

We have recently developed a reverse genetics strategy for inactivating genes in the zebrafish germline[5]. The current zebrafish genome database contains a single *apc* orthologue (Supplementary Fig. 1a, b). We screened an F_1 *N*-ethyl-*N*-nitrosourea (ENU)-mutagenized zebrafish library for apc nonsense mutations mapping to the putative MCR. A premature stop codon corresponding to amino acid (a.a.) 1318 of human APC was identified. The allele was designated apc^{mcr}, and is predicted to constitutively activate Wnt/β-catenin signalling.

apc^{mcr} heterozygotes developed normally. Intercrossing resulted in clutches of F_3 embryos of which 25% died between 72 and 96 hours post-fertilization (h.p.f.), displaying multiple defects. These included, most prominently, cardiac malformation with associated pericardial oedema and blood pooling (Fig. 1b), enlarged otic vesicles, smaller eyes, and body curvature. Further, jaw, pharynx, and inner-ear structures failed to develop and fin buds arrested. Primordia for internal organs such as gut, liver and pancreas formed but developed abnormally (A.F.L.H and A-P.G.H, unpublished observations). Genotyping revealed complete correspondence between this phenotype and homozygosity for the apc^{mcr} mutation. Mutant embryos probably developed beyond gastrulation owing to the presence of maternal Apc (data not shown).

To verify that the above developmental defects were due to loss of Apc function and not to co-segregation of an unidentified linked mutation, we injected zygotes resulting from intercrosses

of *apc*$^{mcr/+}$ heterozygotes with 200 pg of RNA encoding a human APC fragment (a.a. 1020–2032) containing the β-catenin and axin binding domains fused to green fluorescent protein (GFP). We observed a 66% reduction in the expected number of mutants at 48 h.p.f. (23/271 compared to an anticipated 68/271), whereas the expected frequency of mutants was observed in non-injected siblings (24.6%; $n = 167$). Genotyping confirmed that 59.1% of *apc*$^{mcr/mcr}$ homozygotes now appeared phenotypically normal, whereas another 12.5% had normal hearts, but retained most other defects (for example, enlarged otic vesicles, smaller eyes, and body curvature) (Fig. 2c). This implied that the mutant phenotype was due specifically to loss of the Wnt-regulatory function of Apc, and that the heart defects were not secondary to other abnormalities.

In an independent forward genetic screen (D.Z., to be published elsewhere), we identified a second ENU-induced mutant *apc* allele (termed *CA50a*), whose phenotype was indistinguishable from that of the *mcr* mutant (Fig. 1b, d). The *CA50a* allele failed to complement the *mcr* allele. The *CA50a* mutation results in premature stop codon truncation of the encoded gene product at a Leu residue corresponding to position 613 of the human protein.

The heart is the first organ to form and function during vertebrate embryogenesis, and cardiac malformation was the earliest gross developmental defect exhibited by *apc* mutants. Heart morphology, expression of the cardiac marker *nkx2.5*, and chamber specification (ascertained by expression of *cmlc2* and *vmhc*) were all normal at 36 h.p.f. in mutants (data not shown). Mutant hearts comprised both myocardial and endocardial cell layers and initially manifested vigorous, rhythmic peristaltic contractions. Subsequently, however, they failed to undergo looping morphogenesis and contractile function diminished progressively, such that by around 80 h.p.f. both chambers became silent and blood circulation ceased altogether. Prior to this, blood was observed regurgitating within mutant heart chambers (Supplementary videos), indicative of a valve defect. Histological examination and Nomarski microscopy revealed that the discrete endocardial cushions (precursors of the valves proper) positioned between the atrium and ventricle in wild-type hearts had been replaced by a profuse endocardial layer fused at the atrioventricular (AV) boundary in mutant hearts. All endocardial cells appeared to have undergone epithelial–mesenchymal transition (Fig. 1c, d).

In the APC–GFP RNA injection experiment (see above), we observed a class of embryos (6.6%, 18/271) in which hearts failed to undergo looping and blood regurgitated, but that were otherwise morphologically normal at 48 h.p.f. Phase contrast microscopy and histology revealed the absence of endocardial cushions (not shown). These embryos were genotypically wild type (Fig. 2c). Injection of wild-type zygotes with 500 pg of APC–GFP RNA increased the fraction of embryos lacking endocardial cushions at 48 h.p.f. to 11.2% (25/224). This implied that blocking endogenous Wnt/β-catenin signalling could inhibit endocardial cushion formation. To further validate this hypothesis, we injected wild-type embryos with 20 pg of Dkk1 RNA. As reported[6], this resulted in forebrain expansion accompanied by a mild reduction in trunk and tail tissue. Cardiogenesis and vasculogenesis, however, were not compromised (our findings). At 48 h.p.f., we observed a lack of heart looping and blood regurgitation in 33.5% (106/316) of Dkk1-injected embryos, but not in controls (Fig. 2a). Endocardial cushions were absent (Fig. 2b).

Immunohistochemical staining for β-catenin revealed nuclear β-catenin, indicative of activated canonical Wnt signalling[4] in endocardial cells populating the AV cushions and cushions of the bulbous arteriosus of wild-type hearts and the myocardial cells immediately overlying them (Fig. 3a and Supplementary Fig. 2). In

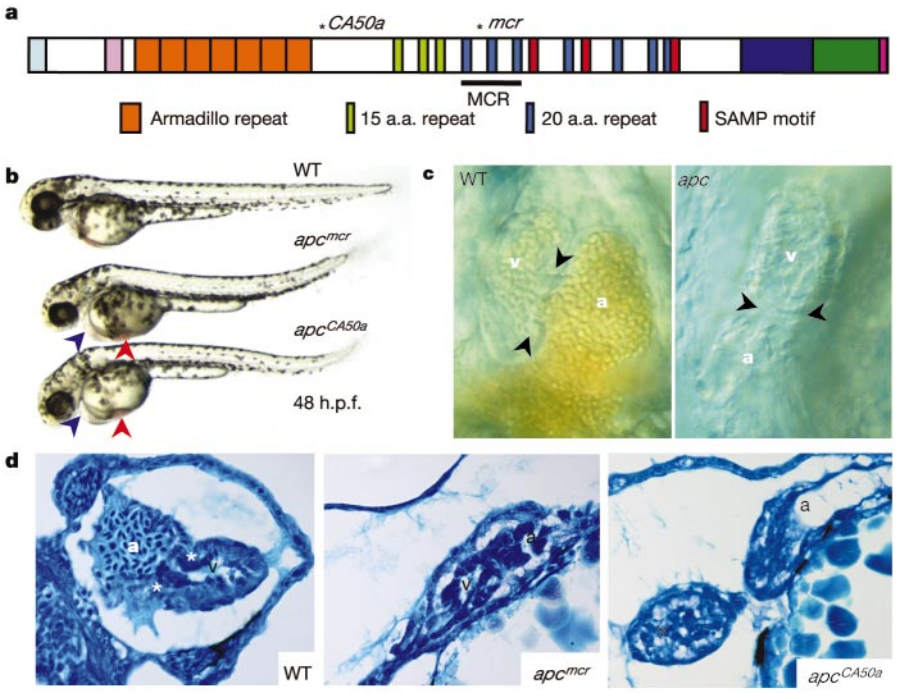

Figure 1 Mutation of *apc* results in heart malformation. **a**, Diagram of wild-type (WT) Apc protein; 15 and 20 a.a. repeats mediating β-catenin binding, and SAMP motifs mediating Axin binding, are depicted. Asterisks indicate the position of the *mcr* and *CA50a* truncations. a.a., amino acid; MCR, mutation cluster region. **b**, Morphology of WT, *apc*$^{mcr/mcr}$ and *apc*$^{CA50a/CA50a}$ embryos at 48 h.p.f. Blue arrowheads indicate pericardial oedema and red arrowheads pooled blood in mutants. **c**, Nomarski microscopy of WT and *apc* hearts at 72 h.p.f. Arrowheads indicate the endocardial cushions in the WT and the fused endocardial layer at the AV boundary in *apc*$^{mcr/mcr}$. **d**, Transverse section of WT and sagittal sections of *apc*$^{mcr/mcr}$ and *apc*$^{CA50a/CA50a}$ hearts at 72 h.p.f. Asterisks indicate endocardial cushions. Note in *apc* hearts the profuse endocardium occluding the aperture between heart chambers and excess cardiac jelly. a, Atrium; v, ventricle.

contrast, all endocardial and myocardial cells within mutant hearts displayed prominent nuclear β-catenin (Fig. 3b). *apc*^{mcr} carriers were crossed with a transgenic zebrafish line expressing GFP under a Tcf responsive promoter (TOPdGFP)[7]. In wild-type embryos we observed GFP expression only within endocardial cushions (Fig. 3c). In *apc* mutant hearts, GFP expression occurred throughout the endo- and myocardium (Fig. 3d). Expression of proliferating cell nuclear antigen (PCNA) mirrored the pattern of nuclear β-catenin, being restricted to transdifferentiated endocardial cells in cushions (Fig. 3e). In mutant hearts, all endocardial cells were PCNA positive (Fig. 3f).

We next examined the hearts of *axin1* mutant (*mbl*) zebrafish[8,9]. Pericardial oedema and blood pooling were observed in the majority (81%; 50/62) of *mbl* mutants. Frequently, this was accompanied by reduced (26%) or absent (13%) looping of the heart tube and blood regurgitation within heart chambers (complete loss of circulation was observed in 7% of *mbl* embryos by 72 h.p.f.). The most severely affected *mbl* mutant hearts closely resembled *apc* mutant hearts (data not shown). *mbl* hearts with intermediate looping displayed enlarged endocardial cushions and a concomitant increase in nuclear β-catenin and PCNA (Supplementary Fig. 3).

To further investigate the link between Wnt/β-catenin signalling and valve formation, we performed *in situ* hybridization (ISH) for *bmp4*, *versican* (or *cspg2*/*br146*) and *notch1b*. As reported previously[10] all three genes are initially expressed throughout the anteroposterior extent of the heart, *bmp4* and *versican* in the myocardium and *notch1b* in the endocardium. Later, expression of these genes is restricted to the AV valve-forming region—*bmp4* and *versican* by 37 h.p.f., and *notch1b* by 45 h.p.f.. At 36 h.p.f., the expression pattern of these three markers was indistinguishable between mutant and wild-type hearts (not shown). By 48 h.p.f., *bmp4* and *versican* expression was restricted to a few myocardial cells at the valve-forming region in wild-type hearts (Fig. 4a, c). In mutant hearts, both genes were dramatically upregulated and the domains of expression greatly expanded, encompassing the entire ventricle (Fig. 4b, d). Likewise, endocardial expression of *notch 1b* was valve-specific in wild-type hearts at 48 h.p.f. (Fig. 4e), but a broader expression domain was detected in mutant hearts (Fig. 4f). At 72 h.p.f., *notch1b* expression was observed throughout the endocardium of mutant hearts (inset Fig. 4f). Another endocardial valve-specific marker, *hyaluronan synthase* 2 (*has2* or *DG42*) (J. Bakkers, personal communication) was restricted to the AV valve-forming region in both wild-type and mutant hearts at 48 h.p.f., albeit already upregulated in mutant hearts (insets Fig. 4g, h). At 72 h.p.f., *has2* expression remained restricted in wild-type hearts (Fig. 4g) but was expressed throughout the endocardium of mutants (Fig. 4h). As *bmp4*, *versican* and *has2* are purportedly transcriptional targets of the Wnt/β-catenin pathway (refs 4, 11, 12, and M. Morkel and W. Birchmeier, personal communication), these data confirmed that Wnt/β-catenin signalling is operative in myocardial and endocardial cells only at the valve-forming region in wild-type hearts.

Cardiac valve formation depends on signalling between myocardial and endocardial cell layers across an elaborate extracellular matrix, involving TGF-β, BMP, and EGF family members[13–15]. Here we uncover a role for the Wnt/β-catenin pathway in this network. Wnt/β-catenin signalling is probably not involved in valve specification. Rather, it regulates subsequent expression of valve markers as well as proliferation and transdifferentiation of endocardial cells to establish endocardial cushions (model in Supplementary Fig. 4). Mice mutant in the Wnt target genes *versican* or *has2* fail to develop endocardial cushions[16,17]. Similarly, *jekyll*

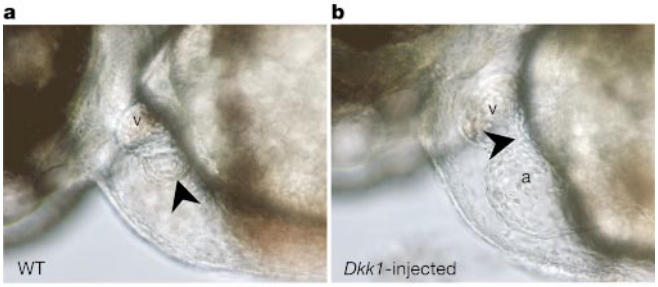

c

Phenotype	Genotype: Sib (%)	Mut (%)
WT	67	15.6
Heart only	0	3.3
Cushion-less	6.6	0
Mutant	0	7.5

Figure 2 Wnt/β-catenin signalling regulates endocardial cushion formation. Lateral views of hearts at 48 h.p.f. in a WT (**a**) and *Dkk1*-injected embryo (**b**). Arrowheads indicate one of the two AV endocardial cushions in **a** and endocardial monolayer at the AV boundary in **b**. a, atrium; v, ventricle; WT, wild type (non-injected control). Anterior to the left. Original magnification ×200. **c**, Percentage of embryos with a given phenotype and genotype following injection of RNA encoding APC–GFP. 'Heart only' denotes rescue of only the heart defect, while 'cushion-less' indicates inhibition of endocardial cushion formation.

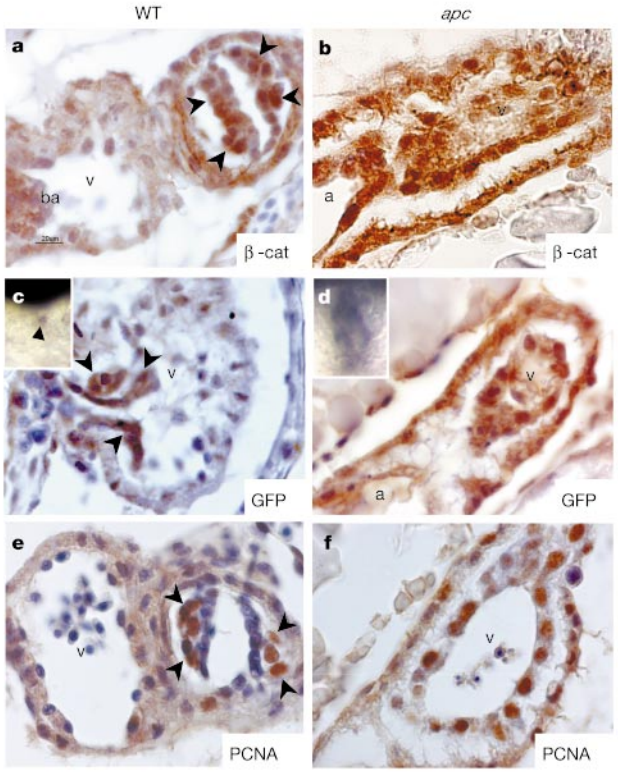

Figure 3 Deregulated Wnt/β-catenin signalling and proliferation in *apc* mutant hearts. Sagittal sections of WT (**a**, **c**, **e**) and *apc* (**b**, **d**, **f**) hearts at 72 h.p.f. stained for β-catenin (β-cat; **a**, **b**), GFP (**c**, **d**) and PCNA (**e**, **f**). Arrowheads (**a**, **c**, **e**) point to positive nuclei (brown precipitate) of transdifferentiated endocardial cells populating AV cushions. Insets in **c** and **d** show whole-mount ISH for GFP expression detected within a few cells only at the AV boundary (arrowhead) in WT;TOPdGFP heart, whereas it is present throughout the anteroposterior extent of the heart in *apc*;TOPdGFP. a, atrium; ba, bulbous arteriosus; v, ventricle. Original magnification ×1,000.

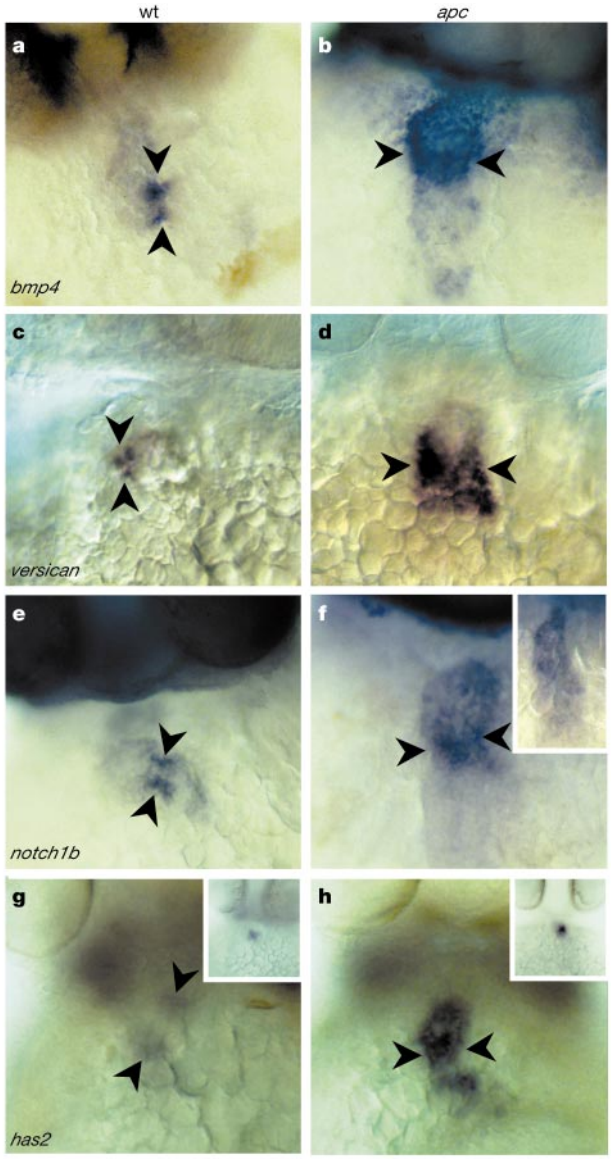

Figure 4 Expression of valve markers is upregulated and expanded in *apc* hearts. Whole-mount ISH of WT (**a**, **c**, **e**, **g**) and *apc* (**b**, **d**, **f**, **h**) embryos at 48 h.p.f. (**a**–**f**, insets of **g** and **h**) and 72 h.p.f. (**g**, **h**, inset of **f**). Myocardial *bmp4* and *versican* expression and endocardial *notch1b* and *has2* expression are restricted to the valve-forming region in WT hearts (arrowheads in **a**, **c**, **e**, **g**), whereas expression of all genes is upregulated and domains expanded throughout the *apc* hearts (arrowheads in **b**, **d**, **f**, **h**). Inset in **f** shows *notch1* expression at 72 h.p.f. Insets in **g**, **h** show *has2* expression being already upregulated at 48 h.p.f. in *apc* hearts. Original magnification ×125.

mutant zebrafish lack functional AV valve tissue. The gene mutated in *jekyll* mutants encodes uridine 5′-diphosphate (UDP)-glucose dehydrogenase[10]. S*ugarless*, the *jekyll* orthologue in *Drosophila*, is required for Wnt signalling[18]. Wnt/β-catenin signalling is therefore probably impaired in *jekyll* mutants. Previously, Wnt/β-catenin signalling has been shown to antagonize cardiogenesis by suppressing cardiomyocyte precursor differentiation from mesoderm[19], demonstrated by conditional deletion of the *β-catenin* gene, which leads to the formation of multiple ectopic hearts[20]. Wnt/β-catenin is also implicated in the proliferation and migration of neural crest cells required for outflow tract septation[21]. Our results now show a distinct role for this pathway in controlling endocardial cell fate decisions and proliferation, thereby modelling the heart proper. □

Methods

Target-selected inactivation of the *apc* gene

Fish embryos were raised and staged as previously described[22]. A sequence contig for the 3′-half of the *apc* gene was constructed by performing database searches in the zebrafish trace database (http://www.ensembl.org/Danio_rerio). We modified a previously described methodology for reverse genetics in zebrafish[5] by incorporating *Cel*I mediated mismatch recognition[23]. Primers (Supplementary Table 1) were designed for the amplification of three overlapping PCR (polymerase chain reaction) fragments (1 kilobase each) and used to screen a library of 4,608 ENU-mutagenized F_1 fish. An F_1 founder harbouring the apc^{mcr} mutation was outcrossed to Ab and TL wild-type backgrounds, yielding identical phenotypes. To identify the *CA50a* mutation, *apc* complementary DNA generated by reverse transcription coupled PCR (primer sequences available on request) on 60 pooled mutant embryos or 60 wild-type siblings was sequenced.

RNA injections

5′-capped mRNAs were synthesized from pCS2+ constructs encoding APC-GFP[24] and zebrafish Dkk1[6] using mMessage mMachine *in vitro* transcription kit (Ambion). RNA in water with 0.2% phenol red was injected into 1–2-cell-stage embryos of Ab or TL strain.

Histology, ISH and immunohistochemistry

Whole-mount ISH was performed as previously described[22]. Probes for *bmp4* and *notch1b* have been previously described[10]. *has2* and *versican* probes were obtained from J. Bakkers. For (immuno-)histochemistry, dehydrated embryos were paraffin-embedded and sectioned at 6 μm. Methylene blue was used for routine histology. Immunohistochemical staining with antibodies for β-catenin (Transduction Laboratories) and PCNA (PC10; Euro Diagnostica) were as previously described[4]. GFP protein was detected using antibody B-2 (Santa Cruz Biotechnology). Serial sections were mounted on the same slide, allowing direct comparison of sections. Visualization was with HRP and DAB.

Received 7 July; accepted 18 August 2003; doi:10.1038/nature02028.

1. Fodde, R., Smits, R. & Clevers, H. APC, signal transduction and genetic instability in colorectal cancer. *Nature Rev. Cancer* **1,** 55–67 (2001).
2. Fodde, R. *et al.* A targeted chain-termination mutation in the mouse Apc gene results in multiple intestinal tumors. *Proc. Natl Acad. Sci. USA* **91,** 8969–8973 (1994).
3. Mao, B. *et al.* LDL-receptor-related protein 6 is a receptor for Dickkopf proteins. *Nature* **411,** 321–325 (2001).
4. van de Wetering, M. *et al.* The beta-catenin/TCF-4 complex imposes a crypt progenitor phenotype on colorectal cancer cells. *Cell* **111,** 241–250 (2002).
5. Wienholds, E., Schulte-Merker, S., Walderich, B. & Plasterk, R. H. Target-selected inactivation of the zebrafish rag1 gene. *Science* **297,** 99–102 (2002).
6. Hashimoto, H. *et al.* Zebrafish Dkk1 functions in forebrain specification and axial mesendoderm formation. *Dev. Biol.* **217,** 138–152 (2000).
7. Dorsky, R. I., Sheldahl, L. C. & Moon, R. T. A transgenic Lef1/beta-catenin-dependent reporter is expressed in spatially restricted domains throughout zebrafish development. *Dev. Biol.* **241,** 229–237 (2002).
8. Heisenberg, C. P. *et al.* A mutation in the Gsk3-binding domain of zebrafish Masterblind/Axin1 leads to a fate transformation of telencephalon and eyes to diencephalon. *Genes Dev.* **15,** 1427–1434 (2001).
9. van de Water, S. *et al.* Ectopic Wnt signal determines the eyeless phenotype of zebrafish masterblind mutant. *Development* **128,** 3877–3888 (2001).
10. Walsh, E. C. & Stainier, D. Y. UDP-glucose dehydrogenase required for cardiac valve formation in zebrafish. *Science* **293,** 1670–1673 (2001).
11. Kielman, M. F. *et al.* Apc modulates embryonic stem-cell differentiation by controlling the dosage of beta-catenin signaling. *Nature Genet.* **32,** 594–605 (2002).
12. Willert, J., Epping, M., Pollack, J. R., Brown, P. O. & Nusse, R. A transcriptional response to Wnt protein in human embryonic carcinoma cells. *BMC Dev. Biol.* **2,** 8 (2002).
13. Brown, C. B., Boyer, A. S., Runyan, R. B. & Barnett, J. V. Requirement of type III TGF-beta receptor for endocardial cell transformation in the heart. *Science* **283,** 2080–2082 (1999).
14. Kim, R. Y., Robertson, E. J. & Solloway, M. J. Bmp6 and Bmp7 are required for cushion formation and septation in the developing mouse heart. *Dev. Biol.* **235,** 449–466 (2001).
15. Iwamoto, R. Heparin-binding EGF-like growth factor and ErbB signaling is essential for heart function. *Proc. Natl Acad. Sci. USA* (2003).
16. Mjaatvedt, C. H., Yamamura, H., Capehart, A. A., Turner, D. & Markwald, R. R. The Cspg2 gene, disrupted in the hdf mutant, is required for right cardiac chamber and endocardial cushion formation. *Dev. Biol.* **202,** 56–66 (1998).
17. Camenisch, T. D. *et al.* Disruption of hyaluronan synthase-2 abrogates normal cardiac morphogenesis and hyaluronan-mediated transformation of epithelium to mesenchyme. *J. Clin. Invest.* **106,** 349–360 (2000).
18. Hacker, U., Lin, X. & Perrimon, N. The *Drosophila* sugarless gene modulates Wingless signaling and encodes an enzyme involved in polysaccharide biosynthesis. *Development* **124,** 3565–3573 (1997).
19. Tzahor, E. & Lassar, A. B. Wnt signals from the neural tube block ectopic cardiogenesis. *Genes Dev.* **15,** 255–260 (2001).
20. Lickert, H. *et al.* Formation of multiple hearts in mice following deletion of beta-catenin in the embryonic endoderm. *Dev. Cell* **3,** 171–181 (2002).
21. Kioussi, C. *et al.* Identification of a Wnt/Dvl/beta-Catenin→Pitx2 pathway mediating cell-type-specific proliferation during development. *Cell* **111,** 673–685 (2002).
22. Westerfield, M. *The Zebrafish Book* (Univ. Oregon Press, Salem, Oregon, 1995).
23. Colbert, T. *et al.* High-throughput screening for induced point mutations. *Plant Physiol.* **126,** 480–484 (2001).
24. Miller, J. R. & Moon, R. T. Analysis of the signaling activities of localization mutants of beta-catenin during axis specification in *Xenopus*. *J. Cell Biol.* **139,** 229–243 (1997).

Supplementary Information accompanies the paper on **www.nature.com/nature**.

Acknowledgements We thank R. Dorsky and R. Moon for TOPdGFP fish and the APC–GFP construct; M. Kosters and J. Mudde for library screening; and J. Bakkers, M. Morkel and W. Birchmeier for sharing reagents and observations before publication.

Competing interests statement The authors declare that they have no competing financial interests.

Correspondence and requests for materials should be addressed to H.C. (clevers@niob.knaw.nl).

A receptor kinase gene of the LysM type is involved in legume perception of rhizobial signals

Esben Bjørn Madsen[1], Lene Heegaard Madsen[1], Simona Radutoiu[1], Magdalena Olbryt[1], Magdalena Rakwalska[1], Krzysztof Szczyglowski[2], Shusei Sato[3], Takakazu Kaneko[3], Satoshi Tabata[3], Niels Sandal[1] & Jens Stougaard[1]

[1]*Laboratory of Gene Expression, Department of Molecular Biology, University of Aarhus, Gustav Wieds Vej 10, 8000 Aarhus C, Denmark*
[2]*Agriculture and Agri-Food Canada, SCPFRC, 1391 Sandford Street, London, Ontario NV5 4T3, Canada*
[3]*Kazusa DNA Research Institute, Kisarazu, Chiba, 292-0812, Japan*

Plants belonging to the legume family develop nitrogen-fixing root nodules in symbiosis with bacteria commonly known as rhizobia. The legume host encodes all of the functions necessary to build the specialized symbiotic organ, the nodule, but the process is elicited by the bacteria[1–3]. Molecular communication initiates the interaction, and signals, usually flavones, secreted by the legume root induce the bacteria to produce a lipochitin-oligosaccharide signal molecule (Nod-factor), which in turn triggers the plant organogenic process[4–7]. An important determinant of bacterial host specificity is the structure of the Nod-factor, suggesting that a plant receptor is involved in signal perception and signal transduction initiating the plant developmental response[8,9]. Here we describe the cloning of a putative Nod-factor receptor kinase gene (*NFR5*) from *Lotus japonicus*. *NFR5* is essential for Nod-factor perception and encodes an unusual transmembrane serine/threonine receptor-like kinase required for the earliest detectable plant responses to bacteria and Nod-factor. The extracellular domain of the putative receptor has three modules with similarity to LysM domains known from peptidoglycan-binding proteins and chitinases. Together with an atypical kinase domain structure this characterizes an unusual receptor-like kinase.

Inactivation of receptor genes typically results in a phenotype where mutants are unresponsive towards the signal normally perceived by the receptor. In *Lotus nfr5* mutants are non-nodulating and are unresponsive to inoculation with *Mesorhizobium loti* or application of purified bacterial Nod-factor signal molecules. Root hair deformation and the early physiological changes observed in wild-type plants shortly after application of Nod-factor are undetectable in *nfr5* mutants[10]. In contrast, mycorrhizal symbiosis with the fungus *Glomus intraradices* is normal in the mutants[11], indicating that *NFR5* acts upstream of the common pathway shared between the fungal and bacterial endosymbiotic systems[12]. Together these phenotypic characteristics suggest that NFR5 is required for perception of the Nod-factor signal and subsequent rhizobia-specific activation of the common pathway.

In order to identify and characterize this putative Nod-factor receptor we initiated map-based cloning of the *NFR5* gene. On the genetic map the *NFR5* locus (formerly known as *SYM5*) was positioned to the lower arm of *Lotus* chromosome II between the AFLP markers E33M40-21 and E32M44-13c (ref. 13). The positional cloning strategy for *NFR5* and the physical map is outlined in Fig. 1a–c and described in the Methods. A contig of TAC and BAC clones was assembled using closely linked markers and sequenced as part of the *Lotus* genome-sequencing programme[14]. Subsequent fine mapping located *NFR5* to a 150-kilobase (kb) region delimited by recombination events (Fig. 1b, c). Considering the mutant phenotype, two putative transmembrane receptor kinase genes present among 13 genes in the sequenced region were considered as candidate genes. Sequencing of the two receptor kinase genes in the three *nfr5* alleles identified mutations in one of the genes. We identified an in-frame deletion removing 27 nucleotides in *nfr5-1*, a retrotransposon insertion in *nfr5-2*, and a point mutation leading to

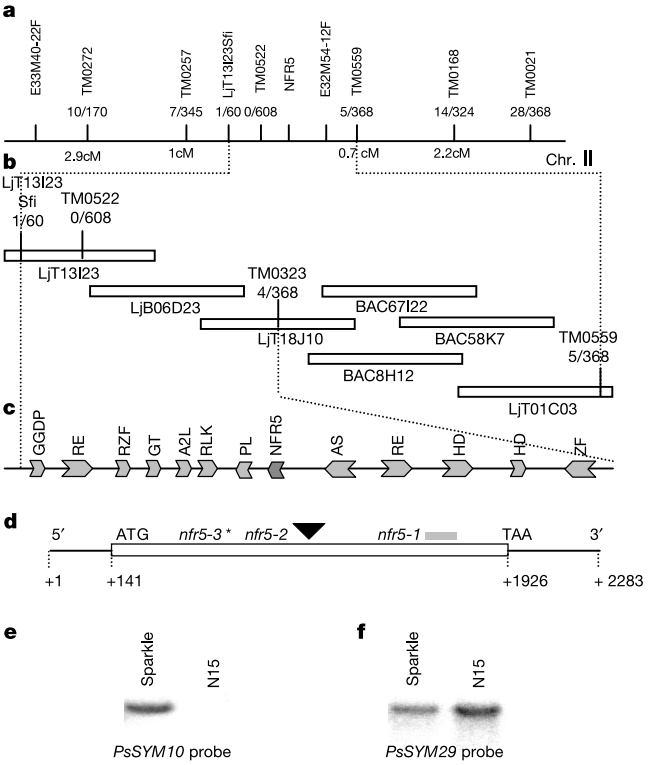

Figure 1 Map-based cloning of *NFR5*. **a**, Genetic map of the *NFR5* region with positions of linked AFLP and microsatellite markers above the line and distances in cM below. The fraction of recombinant plants detected in the mapping population is indicated. **b**, Physical map of the BAC and TAC clones between the closest linked microsatellite markers. The position of sequence-derived markers used to fine map the *NFR5* locus and the fraction of recombinant plants found in the mapping population are indicated. **c**, Candidate genes identified in the sequenced region delimited by the closest linked recombination events. GGDP, geranylgeranyl diphosphate syntase; RE, retroelement; RZF, ring zinc finger protein; GT, glycosyl transferase; A2L, apetala2-like protein; RLK, receptor-like kinase; PL, pectate lyase-like protein; AS, ATPase-subunit; HD, homeodomain protein; ZF, zinc finger protein. Unlabelled, hypothetical proteins. **d**, Structure of the *NFR5* gene, position of the transcription initiation point and the *nfr5-1*, *nfr5-2* and *nfr5-3* mutations. Asterisk, stop codon in *nfr5-3*; black triangle, retrotransposon insertion in *nfr5-2*; grey box, indicates the deletion in *nfr5-1*. **e**, Southern hybridization demonstrating deletion of SYM10 in the N15 *sym10* mutant line. *Eco*RI-digested genomic DNA of the parental variety Sparkle and the fast-neutron-derived mutant N15 hybridized with a pea *SYM10* probe covering the region encoding the predicted extracellular domain. Lack of hybridization with a probe from the 3′ UTR confirmed that the gene was deleted (not shown). **f**, Control hybridization of the same Southern filter using a probe detecting the *P. sativum SYM29* gene[31]. The parental *Eco*RI bands are approximately 5 and 9 kb.